Investigating encapsulation design strategy of photovoltaic cells in the case of a solar race car

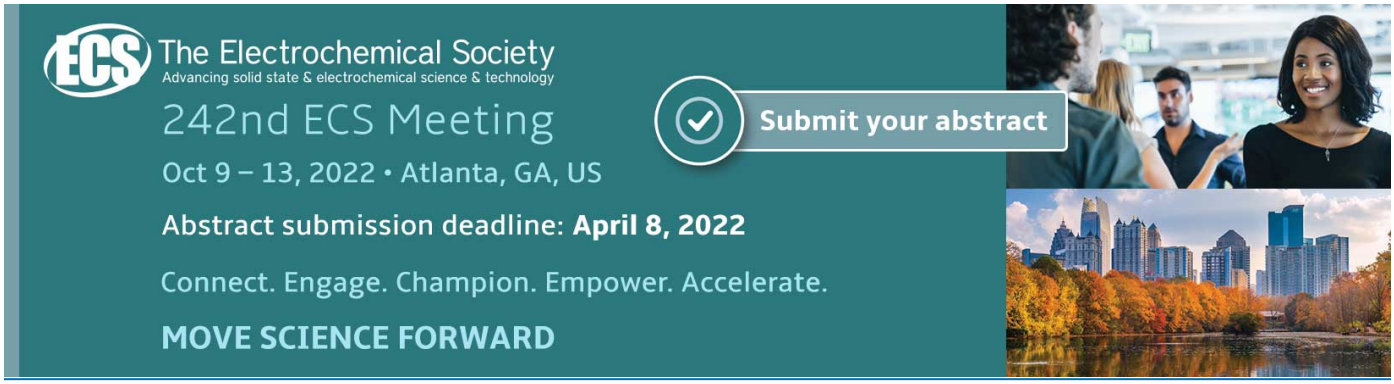

Investigating encapsulation design strategy of photovoltaic cells in the case of a solar race car

A Pavlovic [1*], V Mikhnych [2, 3], M Bertoldi [4] and C Fragassa [1]

[1] University of Bologna (UNIBO), Department of Industrial Engineering, Via Fontanelle 40, Forlì, Italy

[2] Aix-Marseille University, Campus Universitaire de Saint Jérôme, Marseille Cedex 20, 13397 Marseille, France

[3] Karlsruhe Institute of Technology (KIT), Karlsruhe School of Optics & Photonics, Schloßpl. 19, 76131 Karlsruhe, Germany

[4] University of Bologna (UNIBO), Department of Electrical, Energy and Information Engineering "Guglielmo Marconi", Viale del Risorgimento 2, Bologna, Italy

[*] ana.pavlovic@unibo.it

Abstract. The efficiency in converting solar energy into electricity is fundamental wherever photovoltaic panels are present, still more crucial in the design of racing solar vehicles. Even minimal reductions in conversion ratio, maintained for the long solar races, cause solar cars to lose race positions and competitiveness. Here we introduce a numerical-experimental study for choosing the best combination of materials to encapsulate cells in solar roofs. The tangible expectation is to improve the performance of the monocrystalline silicon cells used in our solar vehicle by maximizing heat dissipation to the environment. The operating temperature is in fact a determining factor for efficient conversion, with efficiency drops of the order of 5% every 10 °C. Different stratifications, some of which quite unusual in solar panel design, were compared by transient thermal simulations and experiments. Specifically, five alternatives were analyzed, varying in the presence and thickness of the encapsulation materials (ETFE, EVA and PET). The main scope of the work, however, was not choosing the best among several specific hypotheses, but the development of an accurate numerical model able to predict the behavior of the solar panel in conditions close to the expected ones. This model, in fact, has provided valuable help in optimizing the vehicle design by allowing to evaluate the effect of alternative materials and construction solutions in the cell's construction housing structure.

1. Introduction

For the last few decades, our world has been facing a wide variety of challenges such as climate change, depletion of natural resources and catastrophic fossil fuel impacts. All this resulted in the worldwide

energy crisis [1]. This situation demands an urgent search for sustainable energy technology for the future. Nowadays, there is no doubt that solar energy is destined to be one key energy technology soon. Photovoltaics (PV) is the fastest-growing electrical energy generation source in the world [2] and has undoubtedly a "bright" future. Transition to photovoltaics contributes importantly to environmental protection. Solar energy is renewable energy and can be used in many ways, including solar streetlights, solar mobile batteries, solar buildings, and solar cars. With an increased interest in solar energy, solar cars are coming to the fore.

In order to counteract urban pollution and global warming, electric vehicles are an effective and powerful option. Solar cars refer to the electrical vehicle which is powered by solar energy gained from PV panels that are placed on the roof of the car. The PV module is an interconnected assembly of individual PV cells. Currently, many PV cell types are available in the market. However, because of the high cost, stability, availability of materials, reliability, and lifetime limitations, their widespread availability for commercial applications, such as solar cars, is limited. Besides the above factors, for racing conditions, the conversion efficiency of sunlight into electricity due to light-absorbing materials (such as crystalline silicon, amorphous silicon, gallium arsenide, and organic compounds) remains the most critical parameter [3]. Now, the crystalline silicon PV module is the best choice for onboard electrified vehicles in terms of performance, economy, stability, and availability. The typical efficiency of these cells is about 16%, while commercially this brings about 24% efficiency [4] [5].

In [6] Evans concludes that the efficiency of the PV module decreases by 0,38-0,42% with the temperature growth for silicon cells for one degree. Similar conclusions are also given in [7], which shows a decrease in the total output power of a PV system by 0.4–0.5% under standard test conditions when the module temperature rises by 1°C. In this paper, we are dealing with solar cells, and they have a fundamental effect on the PV module temperature change. Zhou and Yi [8] findings confirm this since the solar cell carried the highest temperature distribution in the PV module.

The current research essentially pursues two goals. The first is to develop a precise three-dimensional finite element (FE) thermal model of five laminated silicon solar cell layups using ANSYS analysis software. FE design helps us predict the actual condition of the PV module under operation and to determine the thermal behavior of each layer of the cell. The second aim is to validate the model by performing infrared (IR) thermography experiments for the same solar cell samples. These two steps will help to obtain the thermal characteristics of the PV module and consequently optimize its performance. For the accuracy of the model, the material, optical and thermal properties of all layers will be well defined. The numerical model with the scope to study photovoltaic modules performance was introduced in [9]. However, in that case, the research was stressed on solar radiation and ambient temperature effect. Furthermore, Chou et al. [10] and Chen et al. [11] studies included similar approaches. Nevertheless, research [10] was focused on the high-concentration PV solar package, while [11] was based on electronic packages.

Literature suggests some recent efforts in thermal modeling of solar cells and PV modules. The study [12] shows that the thermal behavior of the PV module was investigated by applying computational fluid dynamics (CFD) simulation along with the finite element method. Furthermore, to predict the effect of PV module temperature on output power and efficiency, both linear and nonlinear models were developed in [13]. Research [14] proposed a swarm optimization algorithm for calculating the temperature inside the PV module with the relation of the module and electrical efficiency. Moreover, [15] present arguments to emphasize that reducing an operating temperature contributes to a gain in cell and module efficiency. They indicate that operating temperature has a notable impact on the electrical efficiency of the PV module. This finding is supported by [16] who further point out that the temperature rise of the module is a significant issue that influences the efficiency of the solar cell. Moreover, study [17] states that PV cell temperature becomes also one of the key parameters for the long-term performance of the module.

However, none of the reported studies directly combines all specific aspects characterizing the present paper regarding the panel (i.e., monocrystalline silicon, advanced materials for encapsulation, additional layers for structural purposes, material alternatives) and methods (i.e., thermal transient analysis,

absence of CFD dissipative effects, empirical validation). In the present research, several alternative layups of the PV modules were considered with the scope to investigate the effect of design changes in terms of thermal behavior and efficiency, before incorporating them on a solar vehicle [18] [19] [20]. Presented research is continuation of the previously presented paper [21].

2. Materials

2.1. Solar Cells Selection

Currently, monocrystalline silicon solar cells are considered being the best choice for onboard applications for solar vehicles because of their stability, cost, and overall performance. In this research, we use monocrystalline silicon wafer solar cells fabricated by KPE. Provided solar cells have the following main geometrical characteristics:

- Cell area: 125mm x 125mm
- Cell diameter: 150mm
- The shape of the cell: pseudo-square with rounded corners
- Average wafer thickness: 200~220, ± 30μm

At the same time, we consider the additional technical cell dimensions:

- Length of wafer edge: 125mm ± 0.5mm
- Corner to corner minimum / maximum length: 149mm / 151mm
- Flake type chips maximum width / depth: 1.5mm / 0.5mm

We also consider that the number of flake type chips should not exceed 2 per single solar cell. Moreover, monocrystalline silicon is cut from the cylindrical ingots which are grown by the Czochralski process. Because of this, the cell's corners look clipped. The performance of solar cells largely depends on their electrical efficiency. That is why electrical parameters should be also established. In our case, the chosen grade (i.e., PS1) provides a conversion efficiency of 17.25% ± 0.25 while the maximum peak power for the chosen case is 2.56 ± 0.05 Wp. All parameters are measured respecting standard testing conditions: 1,000 W/m^2, AM 1.5G, 25°C.

2.2. Sample composition

The PV module used in our paper comprises an individual solar cell. To preserve the high efficiency and durability, solar cells require corresponding protection which is achieved by a complex mix of various materials. The module is formed by laminating the following layers:

- Frontsheet: ETFE
- Encapsulant: EVA
- Solar Cell: Monocrystalline silicon cell
- Encapsulant: EVA
- Backsheet: PET

This combination was chosen since each material has a property that directly affects the cells' performance.

2.2.1. Frontsheet

The frontsheet typically gives most of the protection, rigidity, and structure for the shape of the cell. Glass is commonly used as a frontsheet in PV modules due to its durability and rather high transmittance. However, in the current layup, we introduced the ETFE material as the frontsheet. ETFE fabricates from a copolymer of ethylene and tetrafluoroethylene resin and afterward extruded into incredibly thin films.

ETFE is a fluorite-based plastic widely applied in the automotive industry that can suffer high temperatures while promoting solar efficiency. This became possible due to the ethene molecule which is extremely stable and allows to withstand high thermal stress and volatile chemicals. In general, the initial function of ETFE was to take over greenhouse glass, and that is why ETFE is lighter and stronger [22]. The major advantages of ETFE compared to glass are weight reduction, extremely high transmissivity, and flexibility of the laminated panel. Essentially, the weight of the ETFE coat is merely 2% of a glass sheet weight. Moreover, the ability of the ETFE to transmit light from ultraviolet to infrared (full light spectrum) brings to an improvement in the efficiency of the entire module. Electric failures are avoided because of the much more efficient insulating power provided by ETFE. The properties such as self-cleanness, excellent electrical resistance, stiffness, resistance to radiation, impact strength and high corrosion resistance make ETFE exceptionally attractive as a frontsheet of a solar cell [23]. Finally, advantage compared to glass is that ETFE is easily recyclable at the end of the solar panel life, and its lightness makes it possible to make a much smaller carbon footprint produced by transportation.

2.2.2. Encapsulant

An essential component of the PV module that produces optical communication, structural support, the thermal conductivity of electrical and physical insulation is an encapsulant [24]. An encapsulant is a material that melts, fully encloses the solar cell and the associated circuitry. Currently, the most used encapsulant in the PV industry is ethylene-vinyl acetate (EVA) copolymer. We chose EVA as an encapsulant since it has good bonding characteristics with our ETFE frontsheet and PET backsheet. EVA links the rest of the layers because of its adhesive nature. At the same time, a thin layer of EVA prevents contamination between the layers since it creates a clean particle-free vacuumed space.

2.2.3. Backsheet

The backsheet is the last layer of material in the PV module. The key tasks of the backsheet are protection, keeping the shape of the entire module and additional insulation of the module from humidity. In this work, polyethylene terephthalate (PET) was taken as a backsheet. PET is plastic based on a fluorine molecule that makes this material very flexible. Such mechanical parameters as exceptionally small Young's modulus and a greater elastic elongation in comparison with other materials prove that PET is one of the best flexible materials at the moment [25]. Afterward, flexibility becomes an extremely critical property for solar cell's subsequent installation into the car's roof. Furthermore, PET refers to those flexible materials that are greatly transparent and show optical transmittance of ~85% over the visible range [26].

2.3. Lamination process

A highly transparent ETFE frontsheet takes a role of a protection layer. ETFE is followed by a thin EVA sheet that spreads all over the frontsheet. We place the EVA layer on the solar cell with the photosensitive surface facing down, while another EVA layer is used to cover the solar cell's backside. Finally, the PET backsheet, which represents an insulating plastic material, is positioned on the second EVA layer.

The next step is a lamination of all layers, which was completed in an autoclave. A plate of glass (removed at the very end) was used to provide planar support for all layers during the autoclaving process. For example, in a standard laminator, the machine worktable takes the function of this glass plate. All pieces were laid on a plate of glass in the following order: PET, EVA, Silicon, EVA, EFTE (Figure 1a).

The entire lamination process takes place in a vacuum in order to overcome the effect of contaminations and penetrating gases. To obtain a vacuum, we used a vacuum bag and a vacuum pump with an applied pressure of 1 bar (Figure 1b). The absence of air helped to achieve structural stabilization of the system and uniform polymerization. For the EVA sheets to polymerize, the plate was heated to 120°C for 90 minutes. Also, the vacuum allows the EVA to be uniformly distributed over the other layers, excluding

the non-functional edges. The following step is cooling (Figure 1c), after which the solar cell is taken out from the vacuum bag. Finally, double-sided tape (cod. 468MP. by 3M) connects to the edges of the entirely laminated solar cell, which subsequently links the solar cell to the carbon fiber composite polymer (CFRP). CFRP is used for the purpose of representing actual conditions since the roof of a solar racing car is made from the same material.

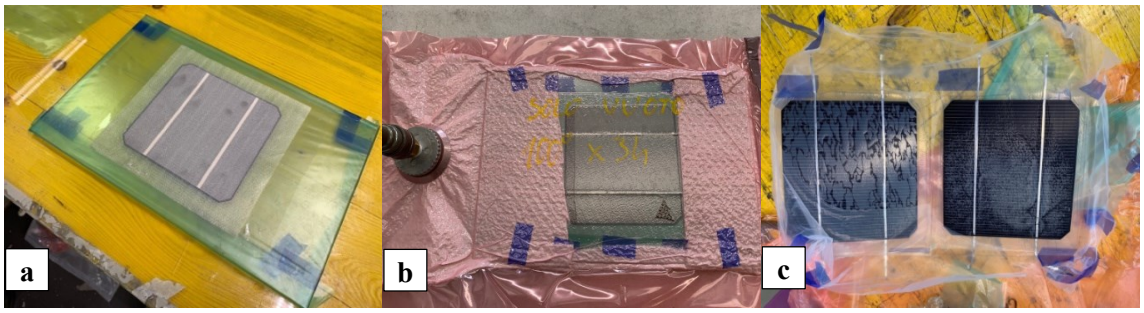

Figure 1. Solar cell lamination process: a) layers stuck (EFTA, EVA, Silicon, EVA, PET) putting on a glass sheet as support for lamination (back view); b) vacuum treatment (1 bar) with a vacuum bug and vacuum pump (back view); c) solar cells after curing in the autoclave (front view).

2.4. Layer Combinations

In this study, we analyzed 5 different layups, which were obtained by removing one or two layers and changing the thickness of the EVA encapsulant (see Table 1).

The first layup involved a complete set of all five layers. Several additional investigations were completed to examine the effect of the various layers on solar cell temperature behavior. Therefore, the second layup was missing the backsheet, while the third layup was tested without the frontsheet. It is necessary to indicate that in all three layups, we used a thick EVA. In comparison, in the fourth layup, we cut down the thickness of the EVA by half (showed as EVA Halved in Table 1). At the same time, in the fifth layup, the thickness of the EVA was diminished by 10 times from the initial thick EVA (EVA thin). In all the aforementioned compositions, double-sided tape and a CFRP plate were used.

Table 1. Variations of layups under investigation.

Layer	Function	Material	Thickness (mm)	Layups				
				1	2	3	4	5
1st	Frontsheet	ETFE	0.28	+	+			+
2nd	Encapsulant 1	EVA Thick	0.2	+	+	+		
		EVA Halved	0.1				+	
		EVA Thin	0.02					+
3rd	Solar Cell	Silicon	0.15	+	+	+	+	+
4th	Encapsulant 2	EVA Thick	0.2	+	+	+		
		EVA Halved	0.1				+	
		EVA Thin	0.02					+
5th	Backsheet	PET	0.2	+		+	+	
6th	Adhesive	Tape	0.13	+	+	+	+	+
7th	Support	CFRP	2	+	+	+	+	+

2.5. Physical and thermal materials' properties

The next essential step was to determine the thermal properties of all materials used. Table 2 illustrates the thermal properties of materials along with references t where they were collected from. With some polymers, properties differed depending on chosen reference and therefore it required a specific choice

(such as an average value). However, the variations between the values were not very significant and thus it did not affect the eventual results of the research.

Table 2. Physical and thermal properties of selected materials.

Material	Density kg/m^3	Thermal Conductivity W/(m·K)	Specific Heat Capacity J/(kg·K)	References
ETFE	1730	0.24	1172	[27] [28]
EVA	945	0.35	2090	[29]
Silicon	2330	148	700	[30] [31] [32] [33]
PET	1350	0.275	1275	[34] [35]
CFRP	1490	6.83	1130	[36]
Tape	1012	0.19	2000	[37]

3. Methods

3.1. Theoretical background

Drawing an analogy between the human body and the solar panel, we state that the sun's rays affect the body in such a way that its temperature becomes greater than the ambient temperature. Parameters such as ambient temperature (T_{amb} in K), specific heat (Q_s in W/m^2), body's absorption coefficient (c_a) determine the thermal equilibrium of the body.

At the same time, if the physical system comprises several layers formed of various materials, it becomes extremely problematic to figure out the overall absorption coefficient. The physical system analyzed in this work is such a system and is illustrated in Figure 2. In this case, it makes sense to describe the thermodynamic problem. Therefore, useful relationships and considerations are given below.

Firstly, induction heat exchange with the external environment is negligible due to the fact that our physical system is closed. The system can be considered closed since the solar panel does not touch the floor, or in other words, our physical system is isolated from the bottom.

Secondly, the following expression is valid for thermal equilibrium:

$$Q_{source} = Q_{conv} + Q_{irr} \tag{1}$$

where $\mathbf{Q_{source}}$ is heat transferred from an energy source to the body.
Q_{irr} - heat emitted by the body through radiation.
Q_{conv} - heat emitted by the body by convection.

Both Q_{conv} and Q_{irr} depend on body temperature (T_{body}) and ambient temperature (T_{amb}).

Newton's Law describes the behavior of convection, which is proportional to the difference between body and ambient temperatures:

$$Q_{conv} = h \cdot \left|T_{body} - T_{amb}\right| \tag{2}$$

where h - the heat transfer coefficient by convection.

At the same time, the behavior of the irradiation is expressed under the Stefan-Boltzmann law:

$$Q_{irr} = A_0 \cdot \sigma_0 \left|{T_{body}}^4 - {T_{amb}}^4\right| \tag{3}$$

where $\boldsymbol{\sigma_0}$ = 5.67 ·10^{-8} W/m^2·k - the *Stefan-Boltzmann constant;* A_0 – exposed area.

The area A_0 is the orthogonal projection of the area of the irradiated body to the angle of the incident rays (a). This area is also referred to the cosine of this angle of incidence defined by Lambert's cosine law. However, we deal with the entire area of the panel since in our experiment $a = 0$ and

cos(a) = 1. Moreover, such physical aspects as the body's geometry, the properties of fluid and air, as well as the conditions of their possible motion are directly related to the coefficient of convection ***h.*** The range of values suitable to the system under test is ***h*** = 2.30-2.75 W/m^2·k. They were determined by making use of parameters such as Nusselt and Grashof numbers. The exact estimation of these parameters can be directly delegated to the simulation code.

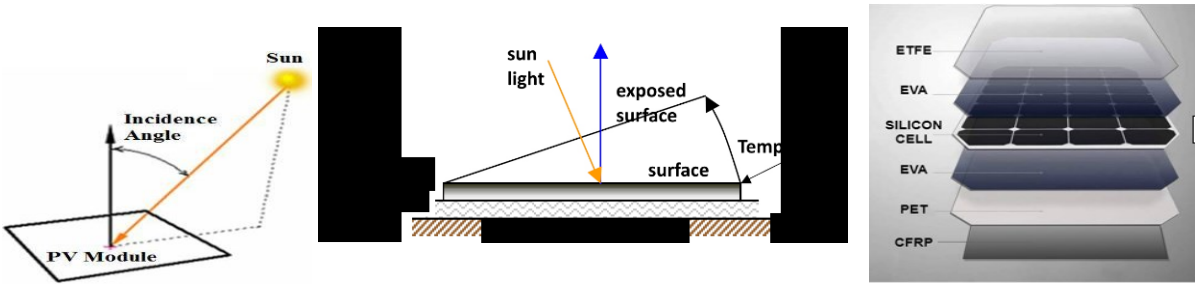

Figure 2. Heat transfer scheme where the radiation acts (with incidence angle ***a***) on a rectangular body in the environment changing its temperature. This body comprises a PV module, made by stratification of different layers (ETFE, EVA, Silicon Cell, EVA, PET), laid on a CFRP panel, before its positioning on supports.

3.1.1. Temperatures

When all additional considerations are identified (geometry, materials, etc.) it is sufficient to apply equations (1)-(3) in order to determine the body temperature ($\mathbf{T_{body}}$), since the heat transmitted by the source ($\mathbf{Q_{source}}$) and the ambient temperature ($\mathbf{T_{amb}}$) in our situation are known (1000 W/m^2 and 25 °C respectively). Furthermore, measuring temperature experimentally is another efficient way to determine $\mathbf{T_{body}}$, which was shown in this work as proof of the simulation results.

As we can observe in figure 2, the solar panel in this work consists of the stratification of various layers, some of which are even transparent. In this regard, it is necessary to clarify what the temperatures from equations (2) and (3) represent.

The surface temperature controls heat transfer, while the change in temperature inside the body is determined by thermal conductivity with a heat flux proportional to the thermal gradient (Fourier's law for thermal conductivity). This ensures the redistribution of heat, which affects the temperature in ways that directly depend on the thermodynamic system. For example, a linear trend between a higher temperature on an exposed surface and a lower temperature on a hidden surface (in the shade) is obtained when the sun's rays are exposed to a homogeneous panel. However, it is highly important to consider that in the case of a solar panel, each layer has its own thermal conductivity, which has a direct impact on the appearance of more complex temperature trends.

3.1.2. Irradiation and diffusion

Concerning the phenomenon of diffusion, the temperature of the outermost layer which is in contact with air serves as the temperature ($\mathbf{T_{body}}$) in equation 2. This wall temperature ($\mathbf{T_{wall}}$) is equivalent to the temperature of the first layer, usually represented by the frontsheet (unless there is no frontsheet in the layup). It is also essential to consider the phenomenon of irradiation. The temperature in equation 3 usually refers to the first layer. However, in our case, the temperature of the silicon is considered to be the wall temperature $\mathbf{T_{wall}}$, since the two layers above silicon (EFTE and EVA) are practically transparent. The silicon temperature relates to the one measured experimentally.

3.2. Numerical simulation

3.2.1. Software and analysis choice

In this research, we established a numerical simulation using the transient thermal analysis in ANSYS Workbench® (Ver. 2020.R2). Since an essential part of the investigation was to determine thermal

variations over time, we preferred transient thermal analysis to a steady-state test. Such thermal factors as temperature distribution, heat fluxes, heat gain or loss, and others characterize thermal analysis. The system also does not undergo fluid dynamics changes such as flowing water or air, so CFD analysis was unnecessary.

3.2.2. Model building

After an appropriate analysis system was chosen, the setup of the model starts with adding materials and specifying their properties. Table 1 and Table 2 show the thickness, mass, thermal conductivity, and specific heat capacity for each layer. The geometry was then created using ANSYS Design Modeler, the computer-aided design (CAD) program used by ANSYS. The geometric model was built by stacking 7 layers of 125x125 mm, and then the corresponding material with the properties already specified in the previous step was added to each of the layers. The layers were assembled with bonded contacts, which ensure the full transmission of forces and heat. In general, the geometry of the simulated sample was reproduced precisely identical to the actual sample up to the clipped corners at the edges (see section 2.1 Solar Cells Selection). In total, five different designs were generated, one per layup.
The next step in the computational analysis was to break up the geometry into pieces in a process called meshing. This discretization was completed with finite elements (FE) in SOLID186. The finite element is a higher-order solid element that exhibits quadratic displacement behavior and is determined by 20 nodes each with 3 degrees of freedom (i.e. nodal displacements along x, y, z). We carried out the discretization of the system for (up to) 198060 nodes and 27702 elements.

3.2.3. Thermal hypotheses

The following hypotheses and conditions were used for the numerical thermal analysis in finite element software to obtain the temperature distribution of the PV module:

- The total irradiance flux of 1000 W/m^2 acts on the panel uniformly and orthogonally.
- The first ETFE layer reflects 7% (= 70 W/m^2) and absorbs 10% (= 100 W/m^2) of the transmitted irradiance.
- The remaining energy (= 830 W/m^2) is not applied on EVA but the silicon cells in the form of constant heat flux.
- Only 3% of the heat flux (= 25 W/m^2) is reflected from the silicon and reaches the ETFE front sheet, while the rest is absorbed by the silicon layer (= 805 W/m^2).
- The transmissivity of the EVA is taken to be unity, which simplifies EVA to fully transparent matter.
- Heat is transferred between sheets by conduction.
- Heat transfer outwards gets through the ETFE and CFRP layers, respecting the phenomena of radiation and convection.
- Transmission and reflection are carried out by silicon layer in the absence of the ETFE frontsheet (3rd and 4th layups).
- For ETFE and CFRP, the emissivity (generally equal to the absorption coefficient corresponding to Kirchhoff's Law) was taken equal to 0.89.
- The convective heat transfer coefficient respectively to the ambient temperature reaches 5.67 W/m^2 °C (e.g. no wind conditions).
- Material properties are temperature independent.

3.3. Experimental validation

To prove the finite element analysis that can predict the temperature distribution of the solar PV module, we additionally performed Infrared Thermography (IRT) measurement. For this test, suitable equipment was used under controlled irradiation and environmental conditions to heat the PV module. At the same time, the temperature was measured over the entire surface of the module. Five different PV module layups (see Table 1) were thermally measured, while each layup measurement was repeated 3 times to achieve precise results. During the examination, all samples were placed on cardboard support on which

solar lamps were directed (see Figure 3). The laminate real-time temperatures were tracked using a FLIR T440® thermal camera with a frame rate of 60 Hz, spectral range between 7.5 and 13 um, and a thermal resolution of 76.800 pixels. This equipment provides thermal and visual imagery, spot size resolution, and reliable temperature measurement even in the transition phase when the sample has not yet reached final equilibrium. The tests were conducted under the standard conditions with an irradiance of 1000W/m^2 and ≈ 24.5°C ambient temperature (varying ±1.5°C). As a result, we discovered a temperature rise over the entire surface of the PV module.

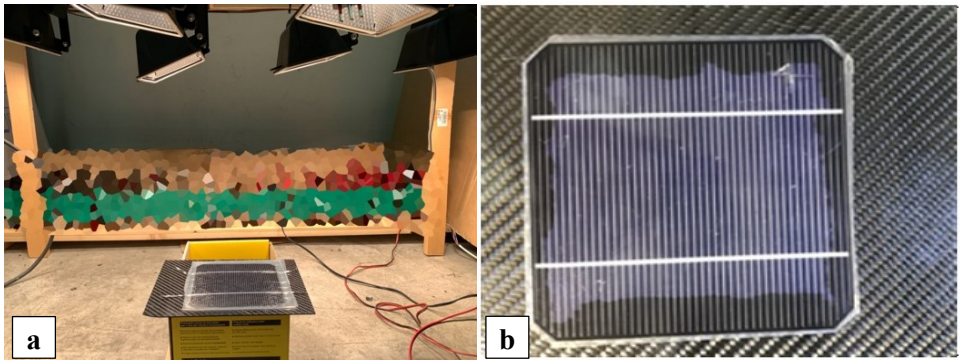

Figure 3. Entirely laminated solar cell under investigation: a) experimental mock-up; b) solar cell.

4. Results and Discussion

4.1. Simulation results

The heat distribution on layers of the laminated solar cells was collected using numerical simulation. In total, 15 tests were completed since 3 evaluations were run for 5 various specimens. In Figure 4, we can identify the temperature propagation over the silicon solar cell (3rd layer) for a 5th layup (absence of backsheet and reduced thickness of EVA). For a visual presentation of temperature propagation, six arbitrary time points were taken (60 sec, 150 sec, 450 sec, 750 sec, 900 sec, 1200 sec). Overall, we can clearly observe the temperature upward trend over time. During the 1st minute, the temperature raised from the ambient temperature (≈ 24.5°C) to 35 °C, while during the next 90 seconds the raise continued and equaled to 11°C. After 450 seconds from the starting point of the test, the temperature reached 65°C, whereas after the first 750 seconds the temperature came to 72°C. The dynamic growth continued resulted in 73.5°C during the following 150 seconds until reaching the equilibrium value (75°C obtained in 1200 seconds).

Moreover, the selected type of analysis helped to realize the heat distribution along each of the layers of the laminated sample independently. Figure 5 illustrates the differences in temperatures between 6 various layers in the case of thermal equilibrium (75°C). The temperature is uniformly distributed over the surface, which does not allow to get details by automatic color scales. This fact makes it practically inconceivable to perform a visual assessment. Due to this reason, the comparison of numeric parameters was done instead of color maps comparison.

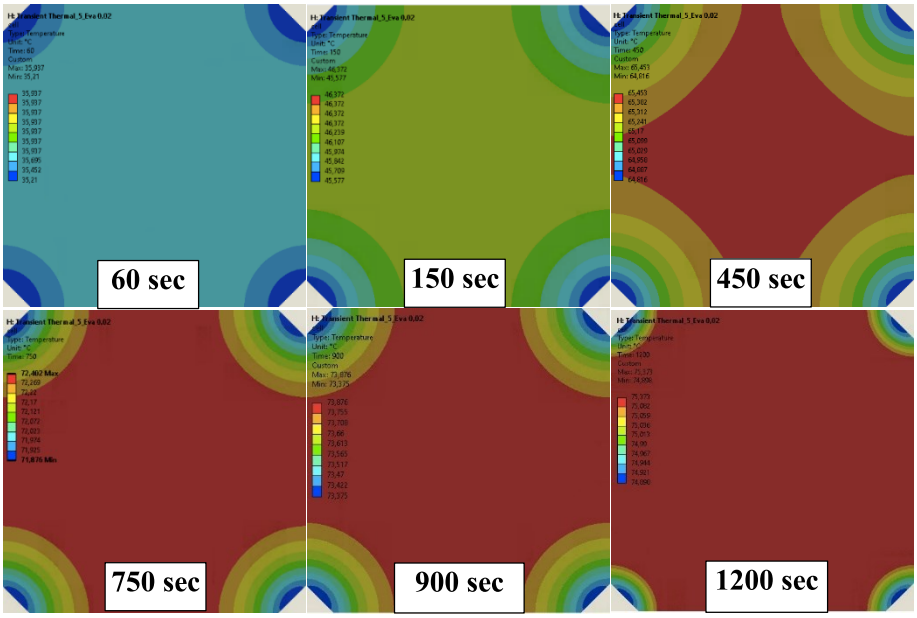

Figure 4. Simulated heat distribution over silicon solar cell layer in 5 arbitrary time points in case of 5th layup: 60 sec, 150 sec, 450 sec, 750 sec, 900 sec and 1200 sec.

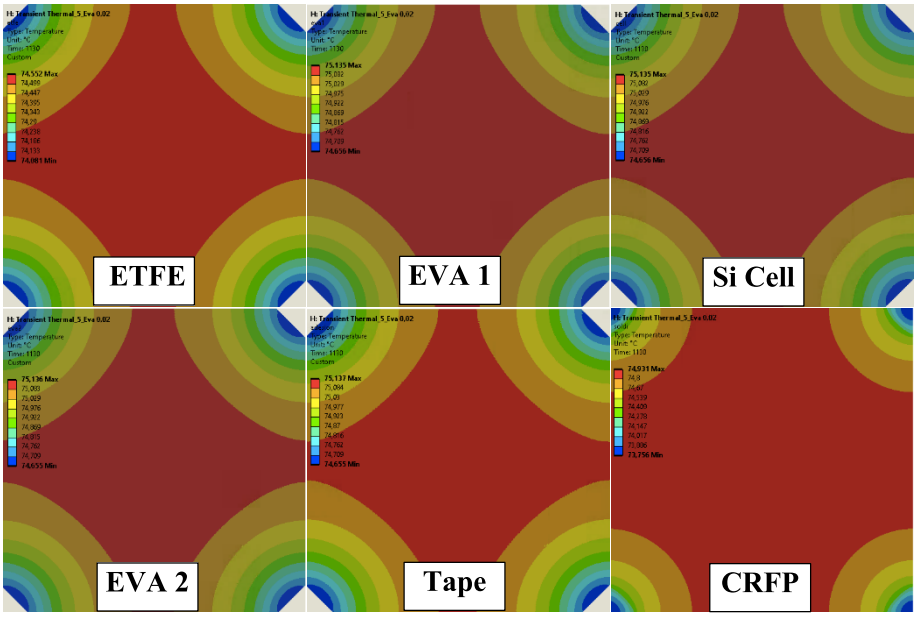

Figure 5. The temperature distribution of each layer of the laminated solar cell at the time of the thermal equilibrium (case of 5th layup, steady state).

The highest temperature values of all layers for various layup options obtained after the simulation are given in Table 3. Additionally, Figure 6 shows the temperature contrast for each layer and each component independently. As a result of the retrieved analytical data, we clearly observe that the peak temperature of the EVA encapsulant does not evolve further than 4 degrees, regardless of the chosen layup. At the same time, as predicted, because of the absence of the frontsheet (3rd and 4th layups), the temperature of the EVA layer came to the maximum values in comparison with the rest of the layups. At the same time, the peak temperature change for double-sided tape and CFRP did not exceed 4.15 degrees. Finally, for the case of the silicon solar cell, we see that the highest temperature varies within 4 degrees from one layer to another.

Table 3. The highest temperatures of all layers detected during the simulation taking into account 5 various layups.

Layer		1st	2nd	3rd	4th	5th	6th	7th
Function		Frontsheet	Encapsulant 1	Cell	Encapsulant 2	Backsheet	Adhesive	Support
Material		ETFE	EVA	Silicon	EVA	PET	Tape	CFRP
Layups	1	67.14	74.12	73.99	74.01	73.90	73.59	73.59
	2	75.40	76.01	77.26	76.25	-	76.08	76.07
	3	-	77.63	77.80	77.81	77.70	77.40	77.40
	4	-	77.87	77.96	77.96	77.96	77.74	77.73
	5	74.56	75.15	75.15	75.14	-	75.15	75.14

Examining the details of heat transitions between layers, we discovered that the maximum temperature with 3rd, 4th and 5th layups fluctuates by less than 1 °C. However, in 2nd layup, the peak temperature contrast between the ETFE frontsheet and the silicon cell reaches approximately 2 °C. Furthermore, by analyzing the peak temperatures between the ETFE sheet and the first EVA layer in the case of the 1st layup, we detected a sharp upsurge of about 7 °C.

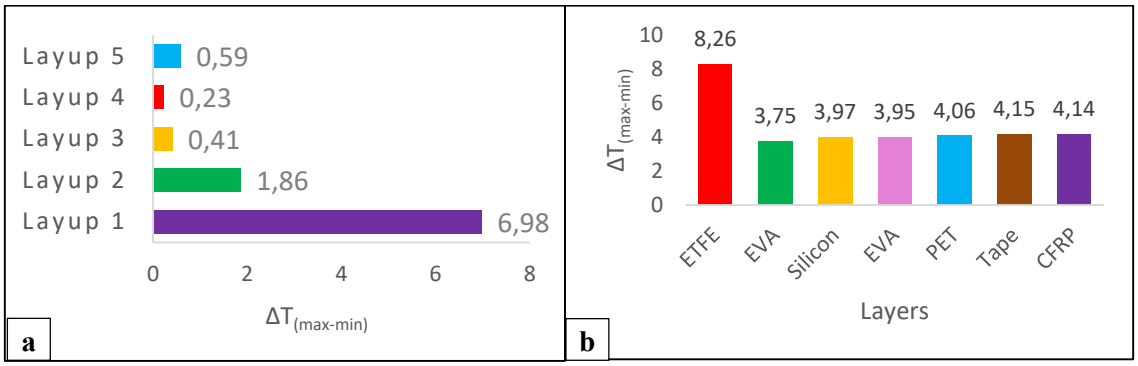

Figure 6. Temperature difference $\Delta T_{(max-min)}$: a) between 7 layers within a single layup; b) between 5 layups within a single layer of the laminated cell.

A direct graphical comparison of the highest temperatures obtained with different layups is displayed in Figure 7a. Here we can see that visually the maximum temperature of the various layers does not change much depending on the layup used. The exception is the 1st layup (or reference layup), considering all 7 layers and with the regular thickness of the EVA layer (0.2 mm), where the ETFE temperature is significantly lower than in the case of other layups (which was already mentioned in the analysis of Table 3). At the same time, Figure 7b illustrates a comparison of the maximum temperatures but in the context of layers of a laminated solar cell. First, because of this analysis, we can certainly see that removing the PET backsheet (2nd layup) has a negative impact on the thermal performance of the entire solar cell, as the temperature of each layer increases compared to a reference sample (1st layup). Second, the established model demonstrates that the layup without the presence of the frontsheet (3rd layup) also adversely affects the temperature of the entire sample. In particular, the temperature of each layer was raised sufficiently by about 4 °C related to the reference layup (except for two EVA sheets, where the maximum temperature increased by ~3.5°C). Next, a drop-off in the EVA thickness by two times (4th layup) basically did not affect the temperature characteristics of the sample, enhancing the maximum temperature of each layer by less than 0.3°C. Finally, considering the absence of the PET backsheet followed by a tenfold cut down in the thickness of the EVA (5th layup), the sample's thermal characteristics were improved (on average 1°C lower T for each layer) compared to an identical specimen with a regular thickness of the encapsulant (2nd layup). Furthermore, it should be noted that the 5th layup is the second most efficient layup after the 1st in terms of temperature characteristics. Except

for the anomalous difference in the maximum temperatures of the ETFE, the temperature of all other layers increased slightly by ~1°C.

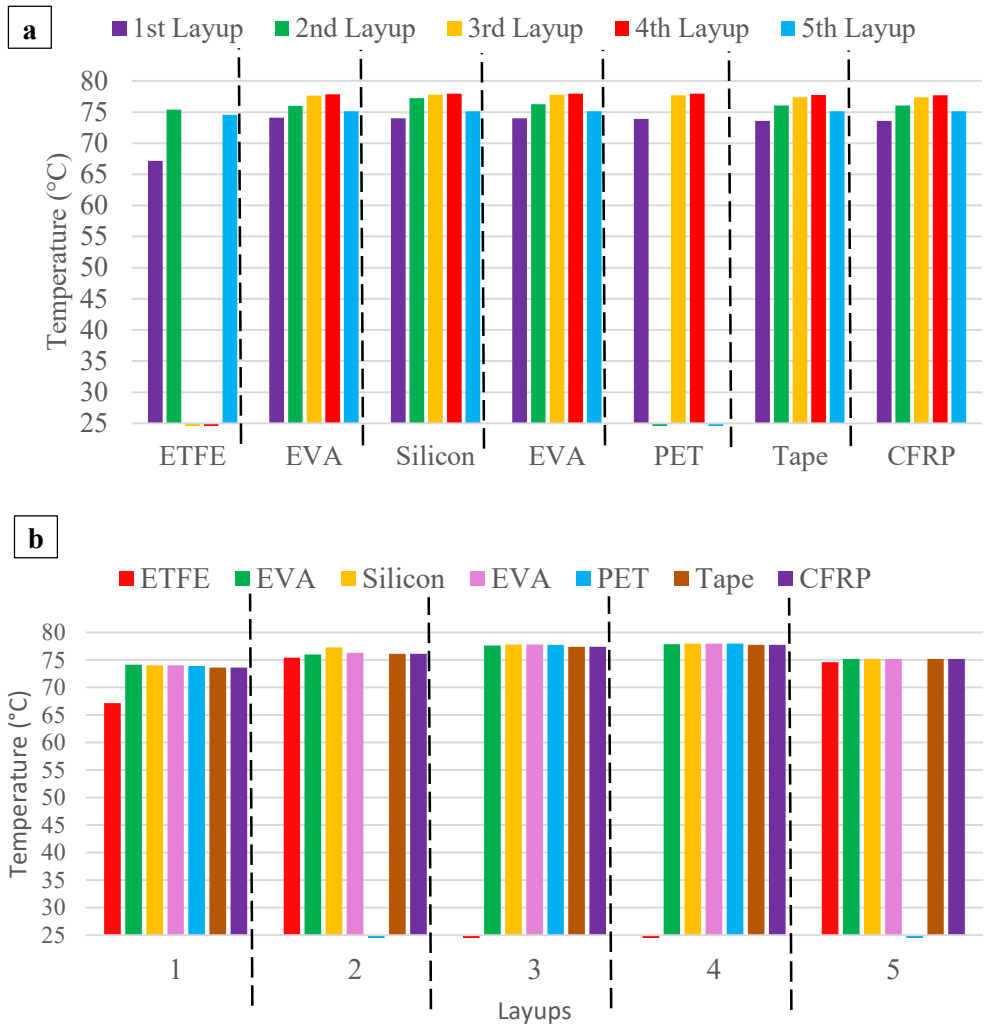

Figure 7. a) Maximum temperatures comparison in terms of different layups; b) maximum temperatures comparison in terms of different layers.

In addition to the classic thermal evaluation of the solar cell, it was essential to assess how one or another layup influences the weight of the fully laminated solar cell and consequently the solar panel weight since it is an extremely crucial parameter of a solar car. That is why the specific weight of the solar cell was determined for all 5 layups. Since the weight is directly proportional to the specific weight of the material (specified in Table 2), it was sufficient to compare the specific weights of the stacked layers of all 5 solar cell variations (see Figure 8) in order to get a full picture of lightness improvement.

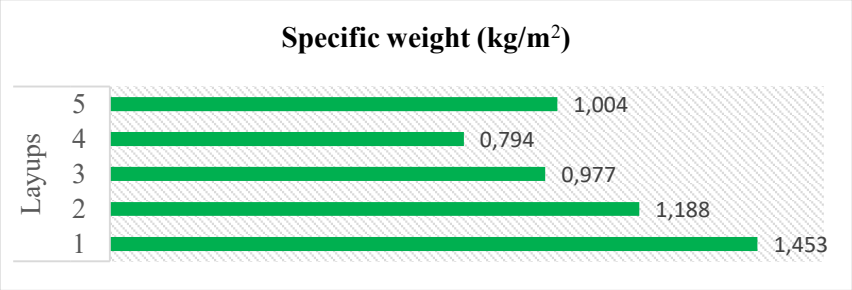

Figure 8. Specific weights of stacked layers in the case of 1st - 5th layups.

According to the results, the ETFE removal in the case of the 2nd layup was followed by a weight reduction of the entire structure by 18.2%. At the same time, a weight decreases of 18.7% was discovered in the absence of an ETFE frontsheet and an EVA thickness cut down from 200mm (3rd layup) to 100mm (4th layup). If the usefulness of running the 2nd layup is still under investigation due to the previously reported rise in the sample temperature, then a twofold loss in the EVA thickness provides a substantial decrease in weight with a minor rise in temperature. Therefore, if weight reduction turns into the primary goal, then applying the 4th layup instead of the 3rd one becomes a relevant choice. Finally, dealing with 5th and 1st layups it can be stated that PET backsheet removal can substantially reduce weight by 40%, accepting the cell's slight temperature rise of 1 °C.

4.2. Experimental results

The results of an infrared thermographic experiment were temperatures measured until the solar sample attained thermal equilibrium. As an illustration of the thermal behavior of the sample during an examination, Figure 9 displays the results of the 5th layup measurements at 5 specific points in time (t = 60 sec, 150 sec, 450 sec, 750 sec, 900 sec) using the FLIR T440 thermal camera. From Figure 9 we can observe that the cross (or probe) was concentrated on the center of the solar cell, where, in theory, the maximum temperature should be focused. This allowed to define the temperature values in the same place and afterward make a corresponding comparison. Also, on the right side of each picture, there is a temperature scale that was set before the start of the experiment. As a result, it allows to compare pictures at different times and visually determine the important heat propagation features over the sample. Further, we assumed all measurements refer to the 3rd and most significant layer of the laminated sample, i.e. the silicon solar cell. This assumption was based primarily on the two following points:

- the initial two layers of the solar cell (ETFE and EVA) are highly transparent.
- simulation results showed that temperature changes between EVA and silicon are minimal.

4.3. Experiment vs simulation comparison

First, as a result of the experiment, it was discovered that the heat flux does not spread uniformly over the surface of the cell, although the opposite was considered during the simulation. In fact, there was a slight shift in heat concentration towards the left part of the sample. This led to a minor deviation from the theoretical data because the maximum temperature moved from the center to other zones of the solar cell. In the end, the difference between the maximum registered temperature and the measurements in the center of the cell came to 5-6°C. However, by measuring and confirming the irradiation value (1000W/m2) at the center of the sample, the effect of inhomogeneity is overcome. Second, it was found that the regularity of the thermal distribution depends on the boundary conditions and local states at the boundaries. Besides this, in accordance with the simulation, the experiment clearly proved that the sample's edge regions are cooled unevenly.

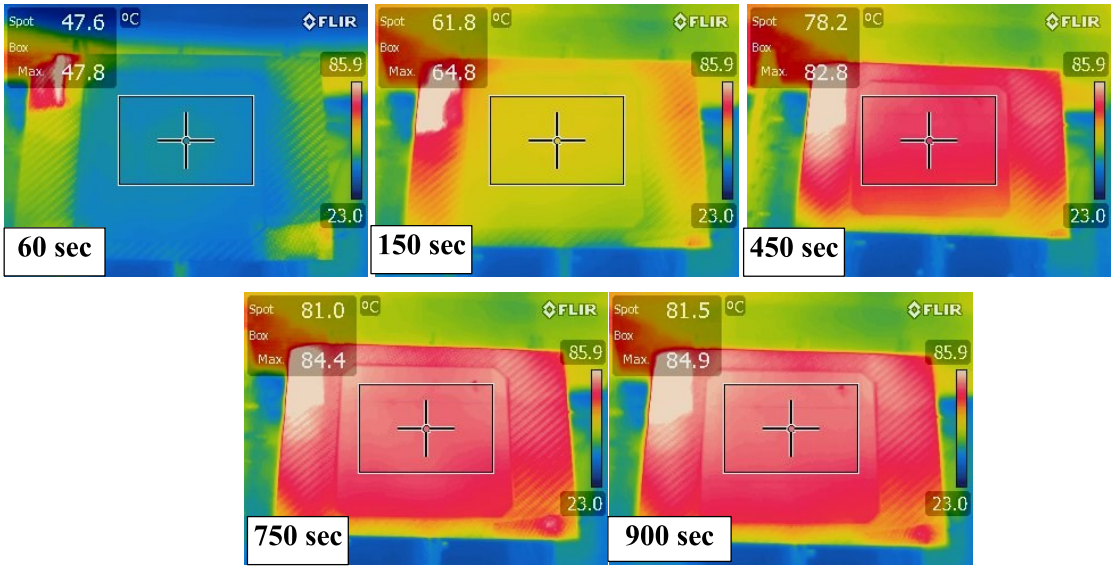

Figure 9. Experiment results: heat distribution over silicon solar cell layer in 5 arbitrary time points in case of 5th layup: 60 sec, 150 sec, 450 sec, 750 sec, 900 sec.

4.4. Thermal steady-state analysis

Figure 10 illustrates a comparison between experimental and simulation results in the case of steady-state conditions for the silicon cell layer. Specifically, 3 empirical tests were completed for each of the 5 layups (tests for a specific layup are marked with the same color, for example, 3 yellow bars in the case of the 2nd layup). In addition, green bars display the finite element simulation results. As a more accurate identification of the data, Table 4 was established, which included the average temperature value for each of the layups. In addition, Table 4 introduces the standard deviation for each layup, as well as the percentage error. It is worth noting that all experimental measures did not undergo strong differences from test to test, as evidenced by a standard deviation of ~1°C for 2nd-4th layups (for 5th layup even reached 0.3°C). However, the deviation value reached 3°C in the case of the 1st layup, which is 4%. Another interesting point is that the average temperature of the silicon layer varied within 10°C, and the greatest variation was recorded between 1st and 5th layups. Eventually, after a direct comparison of the experimental and simulation data, we identified that the simulation predicted the average experimental temperatures with an accuracy of 2.8% in 4 cases out of 5, which is an exceptionally precise result.

Table 4. Differences between empirical temperatures at the midpoint and FEM analysis temperatures at the midpoint.

Layup	Test 1	Test 2	Test 3	Average value	Standard deviation	Simulation Results (FEM)	Percentage error (%)
1st	67.6	72.7	73.4	***71.2***	*±3.2*	**73.2**	2.8
2nd	75.1	74.7	76.1	***75.3***	*±0.7*	**75.4**	0.1
3rd	76.2	77.0	78.3	***77.2***	*±1.1*	**77.8**	0.8
4th	78.7	80.3	80.6	***79.9***	*±1.0*	**78.0**	-2.3
5th	81.2	81.4	81.7	***81.4***	*±0.3*	**75.5**	-7.3

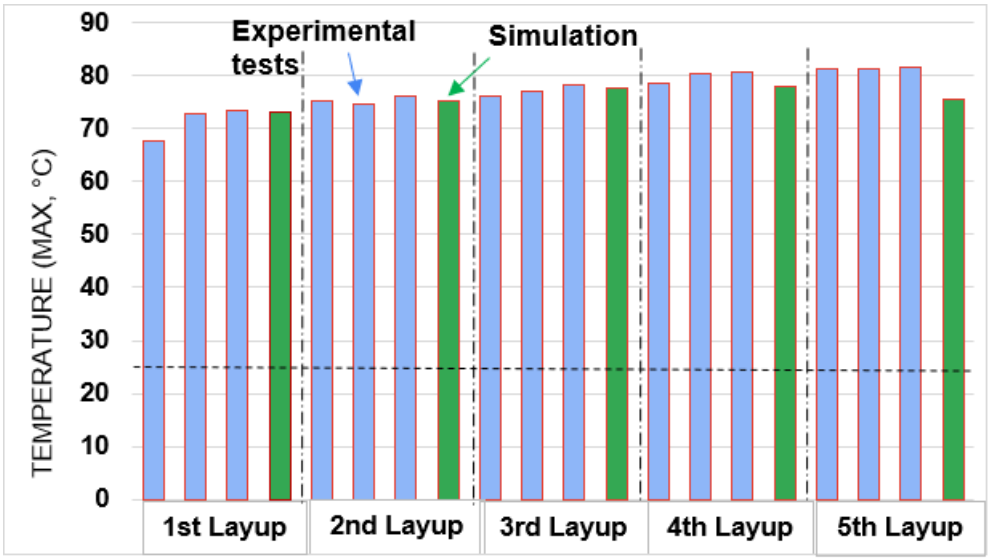

Figure 10. Comparison between experimental (3 tests per layup) and simulation results (1 per layup) in terms of the maximum temperature for each layup.

4.4.1. Thermal transient analysis

Figure 11 depicts a correlation between experimental and simulation results in the case of transient conditions for the silicon cell layer. Like the steady-state investigation, Figure 11 takes into account all 5 possible layups. Analyzing the following graphs, the first factor to note is that practically all experimental curves are superimposed on each other in the case of every layup. This is especially true for the curves of Test 2 and Test 3, which overlap almost perfectly regardless of the selected layup. For the 2nd and 5th layups, empirical curves for all 3 tests are completely overlapped. At the same time, for the 1st, 3rd and 4th layups, the Test 1 curve is located slightly lower than others, which indicates an inclination towards lower temperature values. Since the temperature variations between the tests are not significant (several degrees °C), a variation in the ambient temperature ($\mathbf{T_{amb}}$) can be a rational explanation. The next step is to relate the experimental curves to the curve obtained from the simulation. We observe that in almost all layup options (except for the 5th layup), the analytic curves successfully predict the limiting values of the experimental curves, which was also demonstrated in the steady-state analysis. However, it is crucial to emphasize that significant differences are present in the transition zone. This attitude of the analytic curve may be due to the fact that during the experiment, the system accumulates heat much faster than predicted. Another possible reason for this behavior may be the inability to determine the thermal insulation of the layers under the silicon accurately.

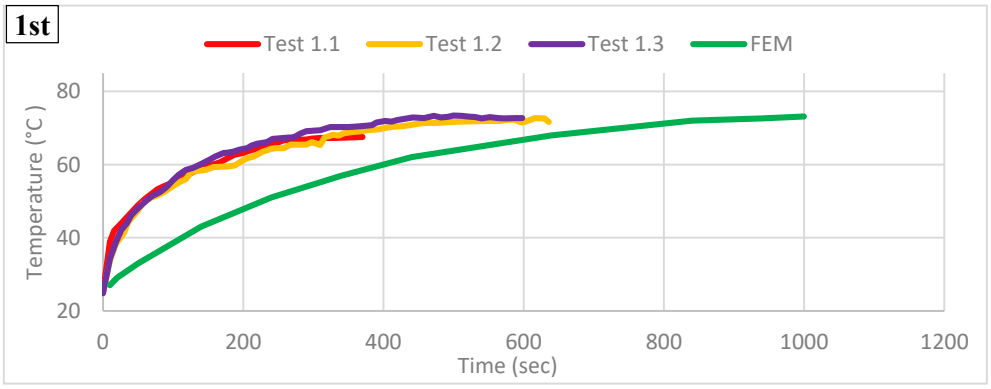

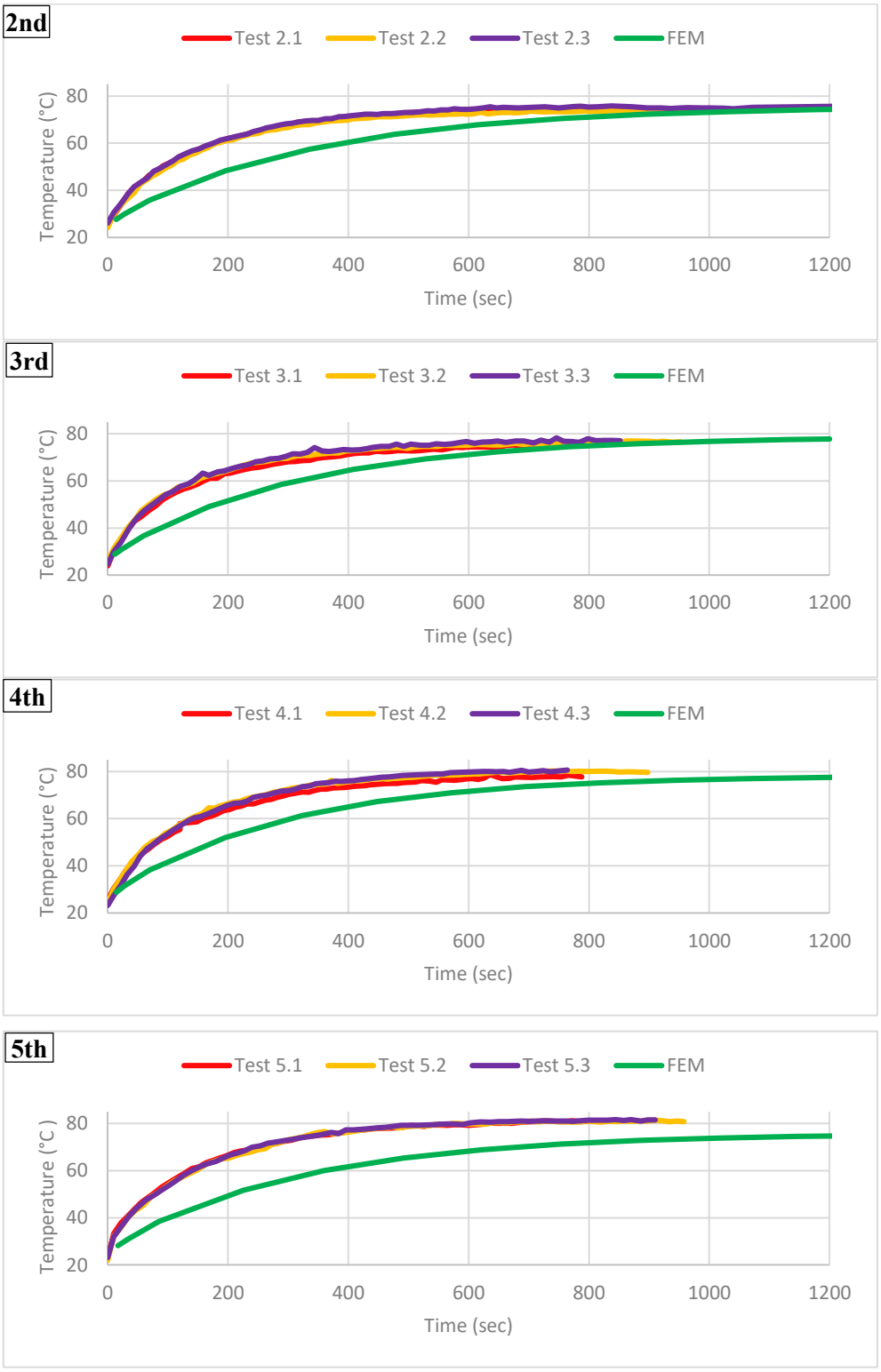

Figure 11. Comparison between experimental (3 tests per layup) and simulation FEM results (1 per layup) in the case of transient conditions.

5. Conclusions

The highest efficiency in solar energy conversion is a fundamental aspect wherever photovoltaic panels

are present, but it is even more critical in the case of racing solar cars. Minimal losses in the conversion efficiency, which however remain present for the many hours of solar racing, can cause the solar car to lose several positions in the standings, especially influencing top vehicles.
The nominal power of photovoltaic panels usually refers to standard test conditions, with solar radiation of 1,000 W/m^2, an air density of 1.5 kg/m^3 and a temperature of the photovoltaic cells of 25 °C. In many cases, however, operational temperature conditions should be considered since the thermal coefficients of the panels can vary considerably. In the case of silicon panels, for instance, this change reaches the highest value between all different technologies, up to 0.5% /°C. It means that the efficiency of the panel can be reduced by 5% every 10 °C of temperature over the standard 25 °C. Therefore, in the presence of cell temperatures of 60°, the drop with respect to the nominal power values can reach up to 17-18%. Here the goal was to improve performance by maximizing thermal dissipation thanks to proper design solutions, involving both the aspects of materials selection and layer thicknesses, for encapsulating monocrystalline silicon solar cells. In this numerical-experimental study, five functional stratifications of monocrystalline silicon cells were made and compared through a transient thermal analysis, validated thanks to experimental temperature measurements.
These results are very promising with a good prediction of temperatures in stationary conditions (less so in transient ones). In some cases, an extreme accuracy was obtained with errors of the order of 0.1-0.8%. Even when lower (7%), the accuracy is enough for an appropriate model utilization.
This kind of information allows finding the right compromise in the cell layup design between the lowest temperature on the cells able to guarantee the highest conversion efficiency and the structural lightness, which cannot be reduced at will, given the functional purposes of each material layer. For instance, it was possible to conclude that a remarkable design option consists in the removal of the last layer (i.e., PET backsheet) to significantly lighten (-40%) the solar panel. This is possible only if the panel is properly inserted in the vehicle design [38] [39] considering convenient support and protective structure (Figure 12).

Figure 12. Solar cars recharging batteries in a pit-stop during the American Solar Challenger: our vehicle is on the right.

The aim of the work, however, was not so much to choose the best among the specific construction hypotheses of the photovoltaic modules investigated here, but above all to set up an efficient numerical model for solar cell design. Thanks to this new validated model it is now possible to easily investigate the behavior of the alternative solar panels in conditions closer to the ones expected from reality. In this sense, different and more complex boundary conditions are awaited in the case of the solar vehicle such as the true three-dimensional geometry of the roof, the angle of incidence of the sun in its different positions, the presence of EV modules side by side, airspeeds while the vehicle is moving. Moreover, in terms of vehicle design optimization, the new numerical model allows to verify the effect of aspects such as the use of different geometries and materials in the solar panel housing structure, as well as the actual usefulness of different passive and active cooling hypotheses proposed by the designers.

6. References

[1] Zendehdel M, Yaghoobi Nia N and Yaghoubinia M 2020 Emerging Thin Film Solar Panels. Reliability and Ecological Aspects of Photovoltaic Modules.
[2] Pvps Iea 2018 Snapshot of global photovoltaic markets. Report IEA PVPS T1-33.
[3] Minak G, Fragassa C, and de Camargo F V 2017 A brief review on determinant aspects in energy efficient solar car design and manufacturing. In International Conference on Sustainable Design *and Manufacturing*, 847-856.
[4] Abdelhamid M, Singh R, Qattawi A, Omar M, and Haque I 2014 Evaluation of on-board photovoltaic modules options for electric vehicles. IEEE Journal of Photovoltaics, 4(6): 1576-1584.
[5] Abdelhamid M 2014 Comparison of an Analytical Hierarchy Process and Fuzzy Axiomatic Design for Selecting Appropriate Photovoltaic Modules for Onboard Vehicle Design. Int. J. Mod. Eng., 15: 23–35.
[6] Evans D L 1981 Simplified method for predicting photovoltaic array output. Sol. Energy, 27: 555–60.
[7] Alami A H 2014 Effects of evaporative cooling on efficiency of photovoltaic modules. Energy Conversion and Management, 77: 668-679.
[8] Zhou J, Yi Q, Wang Y and Ye Z 2015 Temperature distribution of photovoltaic module based on finite element simulation Sol. Energy, 111: 97–103.
[9] Usama Siddiqui M, Arif A F M, Kelley L and Dubowsky S 2012 Three-dimensional thermal modeling of a photovoltaic module under varying conditions Sol. Energy, 86: 2620–31.
[10] Chou T-L, Shih Z-H, Hong H-F, Han C-N and Chiang K-N 2012 Thermal Performance Assessment and Validation of High-Concentration Photovoltaic Solar Cell Module IEEE Trans. Compon. Packag. Manuf. Technol., 2: 578–86.
[11] Chen W-H, Cheng H-C and Shen H-A 2003 An effective methodology for thermal characterization of electronic packaging IEEE Trans. Compon. Packag. Technol., 26: 222–32.
[12] Acanski M, Popovic-Gerber J and Ferreira B 2010 Thermal modeling of the module integrated DC-DC converter for thin-film PV modules Proc. 14th Int. Power Electron. Motion Control Conf. EPE-PEMC 2010.
[13] Pantic L S, Pavlović T M, Milosavljević D D, Radonjic I S, Radovic M K and Sazhko G 2016 The assessment of different models to predict solar module temperature, output power and efficiency for Nis, Serbia Energy, 109: 38–48.
[14] Sánchez Barroso J C, Barth N, Correia J P M, Ahzi S and Khaleel M A 2016 A computational analysis of coupled thermal and electrical behavior of PV panels Sol. Energy Mater. Sol. Cells.,148: 73–86.
[15] Skoplaki E and Palyvos J A 2009 On the temperature dependence of photovoltaic module electrical performance: A review of efficiency/power correlations Sol. Energy., 83: 614–24.
[16] Chou T-L, Shih Z-H, Hong H-F, Han C-N and Chiang K-N 2007 Investigation of the thermal performance of high-concentration photovoltaic solar cell package. International Conference on Electronic Materials and Packaging, 1–6.
[17] Mavromatakis F, Kavoussanaki E, Vignola F and Franghiadakis Y 2014 Measuring and estimating the temperature of photovoltaic modules Sol. Energy., 110: 656–66.
[18] Minak G, Brugo T M, Fragassa C, Pavlovic A, de Camargo F V and Zavatta N 2019 Structural Design and Manufacturing of a Cruiser Class Solar Vehicle J. Vis. Exp. JoVE.
[19] Pavlovic A, Sintoni D, Fragassa C and Minak G 2020 Multi-Objective Design Optimization of the Reinforced Composite Roof in a Solar Vehicle Appl. Sci., 10: 2665.
[20] Pavlović A, Sintoni D, Minak G and Fragassa C 2020 On the modal behaviour of ultralight composite sandwich automotive panels Compos. Struct., 248: 112523.

[21] Pavlovic A, Fragassa C, Bertoldi M and Mikhnych V 2021 Thermal Behavior of Monocrystalline Silicon Solar Cells: A Numerical and Experimental Investigation on the Module Encapsulation Materials J. Appl. Comput. Mech., 7: 1847–55.
[22] Llorens J 2015 Fabric Structures in Architecture.
[23] Burton W S and Noor A K 1997 Structural analysis of the adhesive bond in a honeycomb core sandwich panel Finite Elem. Anal. Des., 26: 213–27.
[24] Czanderna A W and Pern F J 1996 Encapsulation of PV modules using ethylene vinyl acetate copolymer as a pottant. A critical review Sol. Energy Mater. Sol. Cells 43.
[25] Li X, Li P, Wu Z, Luo D, Yu H-Y and Lu Z-H 2021 Review and perspective of materials for flexible solar cells Mater. Rep. Energy, 1: 100001.
[26] Lee C, Park A, Cho Y, Park M, Lee W I and Kim H W 2008 Influence of ZnO buffer layer thickness on the electrical and optical properties of indium zinc oxide thin films deposited on PET substrates Ceram. Int., 34: 1093–6.
[27] Ethylene Tetrafluoroethylene (ETFE) : MakeItFrom.com.
[28] Tefzel-properties-handbook.pdf.
[29] Ethylene Vinyl Acetate (EVA) : MakeItFrom.com.
[30] Properties of Silicon - El-Cat.com.
[31] France-Lanord A, Merabia S, Albaret T, Lacroix D and Termentzidis K 2014 Thermal properties of amorphous/crystalline silicon superlattices J. Phys. Condens. Matter, 26: 355801.
[32] Abe H, Kato H and Baba T 2011 Specific Heat Capacity Measurement of Single-Crystalline Silicon as New Reference Material Jpn. J. Appl. Phys., 50: 11RG01.
[33] Lee B, Liu J Z, Sun B, Shen C Y and Dai G C 2008 Thermally conductive and electrically insulating EVA composite encapsulant for solar photovoltaic (PV) cell Express Polym. Lett., 2: 357–63.
[34] Polyethylene terephthalate - online catalogue source - supplier of research materials in small quantities - Goodfellow.
[35] 2003 Polyethylene Terephthalate Polyester (PET, PETP) - Properties and Applications - Supplier Data by Goodfellow AZoM.com.
[36] Zheng X, Kim S and Park C W 2019 Enhancement of thermal conductivity of carbon fiber-reinforced polymer composite with copper and boron nitride particles Compos. Part Appl. Sci. Manuf., 121: 449–56.
[37] 3MTM Adhesive Transfer Tape 468MP Technical Datasheet.
[38] Fragassa C, Pavlovic A and Minak G 2020 On the structural behaviour of a CFRP safety cage in a solar powered electric vehicle Compos. Struct., 252: 112698.
[39] Ali H T, Akrami R, Fotouhi S, Pashmforoush F, Fragassa C and Fotouhi M 2020 Effect of the stacking sequence on the impact response of carbon-glass/epoxy hybrid composites Facta Univ. Ser. Mech. Eng., 18: 69–77.

Acknowledgments
This research was carried out within the international collaboration project 'Two Seats for a Solar Car', an intervention funded by the Italian Ministry of Foreign Affairs and International Cooperation (MAECI) with the scope to convert a racing solar car into a solar road vehicle. Methodological and technological results are exploited inside the Central European Initiative framework as part of the ‘Composite for All’ and ‘ATC.EVO’ transfer of technology actions.